This article has been accepted for inclusion in a future issue of this journal. Content is final as presented, with the exception of pagination.

IEEE GEOSCIENCE AND REMOTE SENSING LETTERS 1

Integrating UAV and Ground Panoramic Images for Point Cloud Analysis of Damaged Building

Jyun-Ping Jhan⬢, Norman Kerle, and Jiann-Yeou Rau

Abstract—The effectiveness of damaged building investigation relies on rapid data collection, while jointly applying an unmanned aerial vehicle (UAV) and a backpack panoramic imaging system can quickly and comprehensively record the damage status. Meanwhile, integrating them for generating complete 3-D point clouds (3DPCs) is important for further assisting the 3-D measurement of the damaged areas. During the 2016 Meinong earthquake (Taiwan), the system collected multiview aerial images (MVAIs) and ground panoramic images of two collapsed buildings. However, due to the spatial offsets of the spherical camera result in nonideal panoramic images (NIPIs), an appropriate spherical radius has to be chosen to reduce the distance-related stitching errors. In order to evaluate the impact of using NIPIs for 3-D mapping, the geometric accuracy of the 3-D scene reconstruction (3DSR) and usability of the 3DPCs were assessed. This study introduces the stitching errors of panoramic images, uses sky masks for successful 3DSR, and obtains clean point clouds. It then analyzes the usability of point clouds that were obtained from only NIPIs, only MVAIs, and their integration. The analysis shows that NIPIs have more rapid processing efficiency than their unstitched original images and can increase the completeness of point clouds at the building's lower floor, while MVAIs can reduce the stitching errors of NIPIs to an acceptable range. Therefore, integrating both images is necessary to achieve rapid and complete point cloud generation.

Index Terms—3-D point clouds (3DPCs), earthquake-damaged building, panoramic image, unmanned aerial vehicle (UAV).

I. INTRODUCTION

THE EFFECTIVENESS of postdisaster damaged building investigation relies on quick data acquisition, as well as rapid and accurate 3-D point clouds (3DPCs) generation. Recently, unmanned aerial vehicles (UAVs) have gained attention due to their ability of capturing multiview aerial images (MVAIs) of building roofs and facades for structural damage mapping [1]. Given the maturing of modern photogrammetry and computer vision techniques, the structure-from-motion processing can rapidly generate accurate 3DPCs of MVAIs through camera calibration, 3-D scene reconstruction (3DSR), and dense image matching [2]. The 3DPCs not only can assist damaged areas detection [3], but also
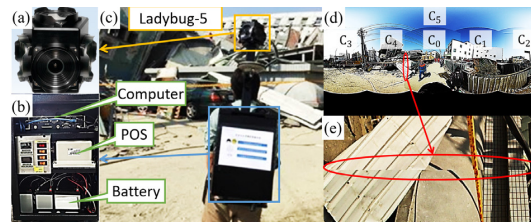
Fig. 1. BPIS and data collection environment. (a) and (b) Ladybug-5 spherical camera and the system overview of the BPIS, respectively. (c) Data collection at a collapsed building. (d) Panoramic image of Ladybug-5 stitched from six images. (e) Stitching error at the boundary of C_0 and C_4.

can be combined with image textures for obtaining accurate and automatic structural damage assessment by applying state-of-the-art object-based image analysis and deep learning methods [4], [5]. However, due to the occlusion of the building itself and surrounding tall structures in densely built-up urban areas, it is difficult to identify the damage status of the building's lower floors in the MVAIs. Although it is possible to operate the UAV manually at low altitude (i.e., <15 m) to observe the lower facade information, this is not an effective way, and it is dangerous when flying at close-range and in narrow alleys.

Conversely, a mobile mapping system [6] that integrates a spherical camera, a position and orientation system (POS), and a computer on a mobile platform (such as vehicle and portable platform) can rapidly access the disaster area, efficiently record the building's lower floor damage status and that of the surrounding environment in ground panoramic images (GPIs), and obtain accurate geolocation information through direct georeferencing [7]. Since a spherical camera can record the entire 360° scene, its utility has been demonstrated in indoor mapping [8] and street view collection [9]. In order to achieve efficient data collection, we utilized a small rotary-wing UAV (DJI Phantom 2) and a portable backpack panoramic imaging system (BPIS) [10] to collect the MVAIs and GPIs of collapsed buildings during the 2016 Meinong Earthquake (Taiwan), and integrated them for 3DPCs analysis.

A. Backpack Panoramic Imaging System

The BPIS integrates a Ladybug-5 spherical camera (by FLIR Integrated Imaging Solutions Inc.), a POS, as well as a computer and batteries in a mountaineering backpack. Fig. 1 provides a system overview of the BPIS and the data collection for a collapsed building, demonstrating how the BPIS can be readily carried by a person in difficult terrain to record building damage. The Ladybug-5 has six wide-angle lenses (labeled as C_0–C_5) that can capture six original images, six undistorted images (UDIs), and one stitched panoramic image.

However, due to the spatial offsets that characterize the multilens system, panoramic image exists stitching errors among overlapping images. The stitching error is principally caused by the distance-related parallax effect, and it can only be ignored when the spatial resolution is larger than the spatial offsets [11]. In close-range environments [see the stitching errors in the red circle in Fig. 1(e)], since the spatial resolution is much higher than the spatial offsets, the collected GPIs are nonideal panoramic images (NIPIs), a proper spherical radius (SR) has to be chosen to reduce the stitching errors. Details of panoramic image stitching are given in Section III.

B. Objectives and Challenges

The suitability of ideal panoramic images for 3-D measurements has previously been demonstrated [12], while a rigorous spherical camera model with spatial offsets has to be considered for NIPIs to obtain accurate 3-D measurements results [13], [14]. However, analysis using NIPIs and appropriate integration with MVAIs for 3DPCs generation remain poorly understood. Meanwhile, Vetrivel *et al.* [4] showed the importance of 3DPCs in assisting deep learning methods for identifying damaged areas, and it is thus necessary to evaluate the impact of stitching errors and analyze the usability of 3DPCs. In this study, six different cases were analyzed to compare the differences of 3DPCs, i.e., NIPIs with three different SR lengths, only UDIs, only MVAIs, and the integration of NIPIs and MVAIs. Therefore, we can 1) analyze the impact of stitching errors in NIPIs by comparing them with the unstitched UDIs; 2) understand how to select the appropriate SR lengths from the best results of NIPIs; and 3) assess the usability of 3DPCs by integrating NIPIs and MVAIs.

In order to obtain reference data for the usability analysis of 3DPCs, we utilize commercial software (Agisoft Metashape) to construct the reference 3-D scene and 3DPCs by integrating MVAIs and unstitched UDIs. Therefore, without using a terrestrial laser scanner to scan more accurate 3DPCs, we can still use dense matching to generate reliable 3DPCs from MVAIs and UDIs for the internal usability assessment. Moreover, it is not possible to obtain the 3DPCs of the building's roof from a terrestrial laser scanner, while MVAIs can obtain them through dense matching. By comparing with the reference data, we analyze the geometric accuracy of 3DSR via the root mean square errors (RMSEs) of ground control points (GCPs), and evaluate the correctness and completeness of 3DPCs. Since placing GCP markers and measuring their coordinates on the collapsed site is dangerous, we marked five stable points, such as building corners and road markings, on the images as reference GCPs, and obtained their coordinates in 3DSR with the assistance of initial positions of the MVAIs and UDIs. In addition, since the UDIs (FLIR) of Ladybug-5 have unreasonable null value areas, and the NIPIs (FLIR) may exist larger stitching errors, we also conducted a camera calibration to obtain reasonable UDIs (Cal.) and NIPIs (Cal.) for the usability analysis.

II. COLLAPSED BUILDINGS OF 2016 MEINONG EARTHQUAKE

On February 6, 2016, an earthquake with a moment magnitude of 6.4 struck southern Taiwan [15], causing numerous
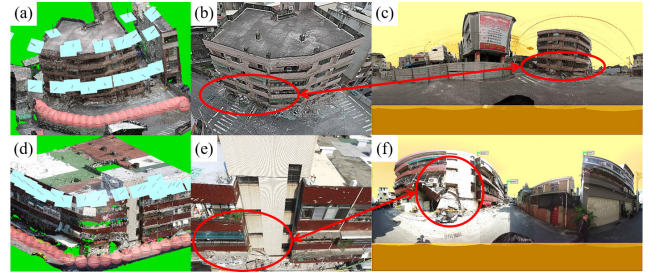

Fig. 2. Image distributions and sample images of the apartment building (top) and the public market (bottom). (a) and (d) 3-D models and image distributions. (b) and (e) Samples of MVAIs. (c) and (f) Samples of GPIs. The red circle shows the viewpoint differences among the MVAIs and GPIs.

buildings to collapse in Tainan city, of which the most serious was the complete collapse of a 17-story residential building, with hundreds of people trapped and 119 fatalities. News media and surveyors responded quickly, who respectively utilized a UAV to acquire video footage and MVAIs for 3-D modeling of the collapsed building. Though the video footage has a lower image resolution than the MVAIs, the comparative quality analysis given by Cusicanqui *et al.* [16] showed that 3DPCs generated from video data possess a geometric quality comparable to those generated from MVAIs.

For the other damaged buildings, including an apartment building and a public market with ground floor failure, we collected their MVAIs and GPIs for conducting the usability analysis of 3DPCs. Fig. 2(a) and (d) shows the 3-D model of the two collapsed buildings, the partial image distribution of MVAIs (cyan) and GPIs (pink), and Fig. 2(b) and (e) shows respective sample images. The red circles depict the viewpoint differences among MVAIs and GPIs, and show that MVAIs can efficiently record the building roof and upper facade, but only GPIs can observe the building's ground floors. The data collection distances of GPIs and MVAIs ranged from 5–10 and 10–50 m, with spatial resolutions of 0.4–0.8 and 0.4–2 cm, respectively.

III. PANORAMIC IMAGE STITCHING AND USABILITY ANALYSIS

Panoramic images can be generated from taking multiple view images and automatic image stitching [17], or can be directly obtained from a calibrated spherical camera. As shown in Fig. 3, a panoramic image results from the 2-D plane and the 3-D spherical coordinate transformation that converts image coordinates (x_i, y_i) to equirectangular coordinates (θ_i, ϕ_i), then to 3-D spherical coordinates (X_s, Y_s, Z_s) with an SR length, and vice versa. According to (1), since the intrinsic parameters and camera rig information of a spherical camera are known and fixed, panoramic image stitching can find the corresponding original image coordinate (x_O, y_O) of each lens from the 3-D spherical coordinates, in which f is the focal length, (Dx, Dy) are the lens distortion corrections, $m_{11}-m_{33}$ are the nine coefficients of rotation matrix derived from relative rotation angles, and (T_X, T_Y, T_Z) are the spatial offsets (1). As the spatial offsets are not zero, this results in SR-related coordinate differences of the same point between two overlapping images, which is the main reason for the stitching errors in the panoramic image. For details about

This article has been accepted for inclusion in a future issue of this journal. Content is final as presented, with the exception of pagination.

JHAN *et al.*: INTEGRATING UAV AND GPIs FOR POINT CLOUD ANALYSIS OF DAMAGED BUILDING
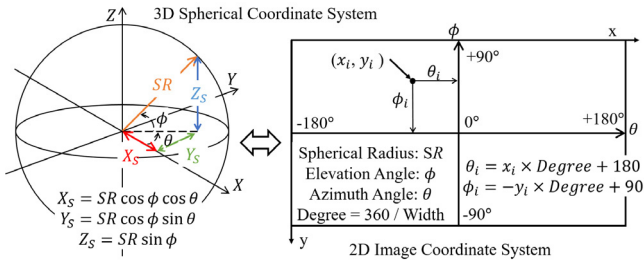
3

Fig. 3. Transformation of 3-D spherical and 2-D image coordinate system.

spherical camera calibration, refer to [10], [18]

$$\begin{bmatrix} x_O \\ y_O \\ -f \end{bmatrix} = \begin{bmatrix} m_{11} & m_{12} & m_{13} \\ m_{21} & m_{22} & m_{23} \\ m_{31} & m_{32} & m_{33} \end{bmatrix} \begin{bmatrix} X_S - T_X \\ Y_S - T_Y \\ Z_S - T_Z \end{bmatrix} + \begin{bmatrix} Dx \\ Dy \\ 0 \end{bmatrix}. \quad (1)$$

The maximum spatial offsets between the lenses of the Ladybug-5 is 10 cm, and the system acquires imagery with a spatial resolution of 0.4 cm at 5 m distance, meaning that the stitching errors can only be ignored when the object distance is larger than 100 m. However, the object distance in the GPIs varies from several to tens of meters, hence it is difficult to choose an appropriate SR length. In order to evaluate the difference of SR, we chose 5, 10, and 20 m for the usability analysis (NIPI-5, NIPI-10, and NIPI-20) of 3DPCs, in which 5 and 10 m are the range of data collection distances, and 20 m is the average object observation distance.

A. 3-D Scene Reconstruction

Due to the differences between the viewpoints of MVAIs and GPIs/UDIs, it is hard to find matches for connecting them and recovering their orientations. Fanta-Jende *et al.* [19] proposed an image-to-plane projection for reducing the viewpoint differences between MVAIs and GPIs, making image matching and coregistration possible. In this present study, in order to have a successful connection between MVAIs and GPIs/UDIs, a higher key point extraction threshold of 50 000 was selected, to increase the chance of matches, while another five manually measured GCPs further assisted the connection. Moreover, false matches in the invalid areas (i.e., sky) of GPIs caused 3DSR failure, also inducing noise in the 3DPCs, hence image processing is necessary to mask the sky areas.

1) Sky Mask: The sky is generally the area with higher blue color values, hence we first used a median filter to smooth the noise within the sky patches, and a Sobel filter to obtain the edges between the sky and other elements. As shown in Fig. 2 (c) and (f), sky areas were then segmented in the GPIs (depicted in orange color) by the region growing of blue color and the edge constrain, while the lower part was covered with a rectangle to mask the null value areas.

2) Accuracy Assessment: Two indices are used to analyze the geometric accuracy of 3DSR through GCPs: the RMSEs of reprojection errors (pix. unit) and the RMSEs of coordinates (cm unit), in which they respectively represent the accuracy of 2-D image measurement and 3-D geolocation.

B. 3-D Point Clouds

3DPCs were generated through dense image matching with 1/2 image resolution (average spatial resolution of 2.5 cm).
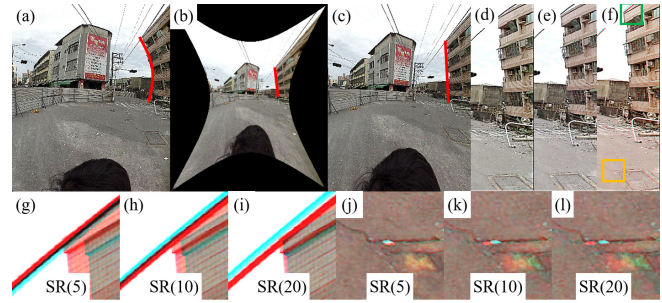

Fig. 4. Comparisons of different UDIs and the stitching errors of panoramic image. (a)–(c) Original image, the UDI (FLIR), and the UDI (Cal.), respectively. (d)–(f) Samples of overlap areas and coregistration result. (g)–(l) Stitching errors of green (farther) and orange (nearer) rectangles with SR length of 5, 10, and 20 m, respectively.

By comparing them with the reference 3DPCs and calculating the cloud-to-cloud distance in CloudCompare software, we obtained the absolute distance differences of the six different 3DPCs, and evaluated their correctness and completeness.

1) Correctness (Corr.): Correctness is the ratio of correct points over all 3DPCs. We choose 5 cm (2 pixels level) as the threshold to consider points with absolute distance smaller than the value are correct, and then calculated the correctness of 3DPCs and applied the filtered points in the subsequent completeness evaluation.

2) Completeness (Com.): Completeness represents the coverage of areas that are sufficiently accurate for damage mapping, which is the percentage of overlapping points with the reference 3DPCs. Since the point density is different, all correct 3DPCs are thinned to the same point density of 2.5 cm × 2.5 cm (1-pixel level), and then estimated the completeness.

IV. RESULTS AND ANALYSIS

This section presents the data processing of GPIs and the results of usability analysis of 3DPCs.

A. Data Processing of GPIs

1) UDIs and Stitching Errors of Panoramic Image: Fig. 4 depicts the differences of UDIs and the stitching errors for different SR lengths. It shows that the red line representing the building boundary in the original image Fig. 4(a) is a curve and was corrected to a straight line in the UDIs [FLIR and Cal., Fig. 4(b) and (c)]. However, since the UDI (FLIR) maintains the same image resolution, the lens distortion correction creates null value areas and loses the details, while the UDI (Cal.) maintains the same pixel size. Thus, a reasonable image can be obtained and used for generating the reference data. Meanwhile, we can observe that the shortest and longest SR lengths lead to the smallest stitching errors at the nearer and the farther objects, respectively, demonstrating that the effects of stitching errors are related to the SR lengths, and that it is hard to choose a proper value via visual observation alone.

2) Data Processing With and Without Sky Mask: The sky mask is the key step for successfully recovering the orientations of GPIs and acquiring clean 3DPCs. Comparing Fig. 5(a) and (b), image matching without the sky mask detects many feature points (white) in the sky area and only yields a few matches (blue), which not only results in the failure of 3DSR

This article has been accepted for inclusion in a future issue of this journal. Content is final as presented, with the exception of pagination.

4   IEEE GEOSCIENCE AND REMOTE SENSING LETTERS
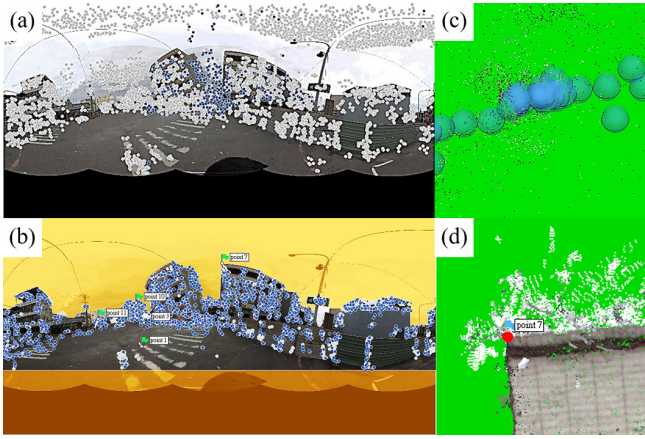

Fig. 5. Challenge of data processing with and without sky mask. (a) and (b) Matches without and with sky mask, respectively. (c) and (d) Failure of 3DSR and noises in 3DPCs, respectively.

TABLE I
GEOMETRIC ACCURACY OF 3DSR

Apartment Building ([1]Ref. 317 images, 75 min.)					
Case	NIPIs: FLIR/Cal.			UDIs	MVAIs	[2]Integration FLIR/Cal.
	5 m	10 m	20 m			
Images	40			240	77	117
RMSEs (cm)	10.3/8.6	5.4/4.3	3.7/2.0	0.5	0.3	1.5/**0.8**
RMSEs (pix.)	2.3/2.3	1.2/1.0	0.7/0.6	0.2	0.2	0.8/**0.6**
Time (min.)	3			9	6	**13**
Public Market ([1]Ref. 297 images, 80 min.)					
Case	NIPIs: FLIR/Cal.			UDIs	MVAIs	[2]Integration FLIR/Cal.
	5 m	10 m	20 m			
Images	40			240	57	97
RMSEs (cm)	12.3/7.5	3.8/2.9	3.9/2.8	0.5	0.4	1.7/**0.7**
RMSEs (pix.)	1.7/1.6	0.7/0.7	0.4/0.4	0.2	0.2	0.4/**0.2**
Time (min.)	3			10	5	**12**
[1]Reference data are generated by integrating UDIs and MVAIs. [2]The result of integrating NIPI-20 and MVAI.						

(compare Fig. 5(c) to Fig. 2(a), the positions of GPIs are unreasonable), but also noises at the boundary of building in the resulting 3DPCs [Fig. 5(d)]. An example of marked GCP (red dot) can also be found in Fig. 5(d).

B. Results of 3DPCs Usability Analysis

1) Geometric Accuracy Assessment of 3DSR: Table I summarizes the geometric accuracy of the six different cases of the two collapsed buildings, which includes the number of images, the RMSEs of GCPs, and the processing time of 3DSR. It shows that the UDIs and MVAIs present an accurate image measurement accuracy of 0.2 pixels and a geolocation accuracy of 0.3–0.5 cm. However, as stitching errors exist in the NIPIs, the image measurement accuracy and geolocation accuracy are respectively 2–11 times (i.e., 0.4–2.3 pixels) and 4–20 times (i.e., 2.0–12.3 cm) worse than those of unstitched UDIs. In the comparison of three different SR lengths, even though NIPIs-5 and NIPIs-10 are the data collection distances that are supposed to have better accuracies, NIPIs-20 achieved the best. This is because of the intersection length between different stations of NIPIs that is actually much longer than 5 and 10 m, which also explains that the longer SR lengths lead to better results. Therefore, the integration analysis adopted NIPIs-20 for the usability analysis of 3DPCs.

TABLE II
CORRECTNESS AND COMPLETENESS OF 3DPCS

Apartment Building (Ref. 1128 k pts)					
Case	NIPIs: Cal.			UDIs	MVAIs	MVAIs & NIPIs-20
	5 m	10 m	20 m			
Corr. (%)	24	43	55	95	83	**80**
Com. (%)	24	41	51	69	82	**92**
Pts (k)	267	467	574	777	926	**1035**
Public Market (Ref. 5375 k Pts)					
Case	NIPIs: Cal.			UDIs	MVAIs	MVAIs & NIPIs-20
	5 m	10 m	20 m			
Corr. (%)	32	38	56	89	96	**82**
Com. (%)	13	18	25	47	69	**76**
Pts (k)	704	962	1364	2546	3713	**4109**

Although the performance of NIPI-20 is unsatisfactory, the integration results with MVAIs are two to four times better, and are improved to a more accurate geolocation accuracy of 0.7–0.8 cm. Meanwhile, since the number of NIPIs is one-sixth that of UDIs, its processing efficiency is not only three times faster compared to UDIs, but also significantly improved the efficiency of integration results by sixfold compared with the reference data that integrating UDIs and MVAIs. Moreover, the NIPIs (Cal.) present a better accuracy than NIPIs (FLIR), demonstrating that NIPIs (FLIR) have larger stitching errors and require camera calibration to yield accurate results. Hence, we adopted NIPIs (Cal.) for the usability analysis of 3DPCs.

2) Correctness and Completeness Evaluation of 3DPCs: The *Cor.*, *Com.,* the number of points (Pts), and the processing time of the 3DPCs are summarized in Table II. The reference 3DPCs of the apartment building and the public market that were generated from integrating MVAIs and UDIs are depicted in Fig. 6(a) and (b). The absolute distance differences of the six cases of the two collapsed buildings are shown in Fig. 6(c)–(n), respectively. Since there are less 3DSR errors in the UDIs and MVAIs, they show correctness of up to 83%–96%, of which the MVAIs of the apartment building have the lowest value. As shown in Fig. 6(g), this is due to the apartment building slants toward the front, which means that the MVAIs do not efficiently observe the building façade, resulting in larger errors. On the other hand, due to the viewpoint differences among UDIs and MVAIs, their completeness (i.e., 47%–69% versus 69%–82%) differs substantially, in which there is a lack of 3DPCs on the roof of ground UDIs and the lower façade of MVAIs, respectively.

Similar to the trend of geometric accuracy assessment, the analysis of different SR lengths shows that the longer SR length has higher usability of 3DPCs, but they have lower values of correctness and completeness, ranging from 24%–56% and 13%–51%, respectively. Compared with the results of unstitched UDIs [Fig. 6(f) and (l)], the results of NIPIs [Fig. 6(c)–(e) and (i)–(k)] present a lower point density, larger errors, and missing blocks in 3DPCs. However, when NIPIs-20 are integrated with MVAIs and compared to the result of the individual data sets, the correctness and completeness of 3DPCs increase to 80%–82%, and 76%–92%, respectively. Focusing on the building facade and the roof in Fig. 6(h) and (n), we can see that the integration can reduce the errors on the building facade (larger number of blue points) of NIPIs-20, although it also introduces additional errors (more green points) on the building roof of MVAIs. Moreover, the

JHAN *et al.*: INTEGRATING UAV AND GPIs FOR POINT CLOUD ANALYSIS OF DAMAGED BUILDING 5

This article has been accepted for inclusion in a future issue of this journal. Content is final as presented, with the exception of pagination.
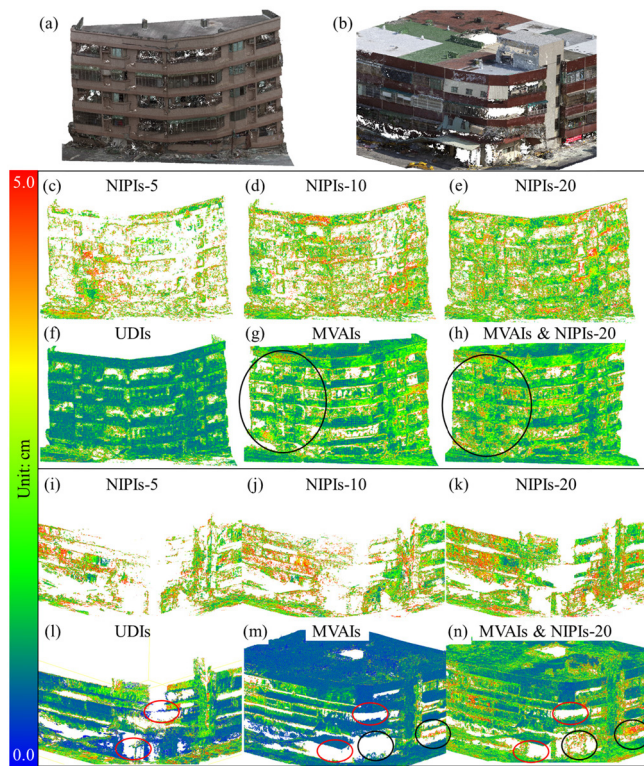

Fig. 6. Reference 3DPCs and absolute distance differences. (a) and (b) Reference 3DPCs of the apartment building and the public market that are generated from MVAIs and UDIs. (c)–(n) Absolute distance differences of six 3DPCs of apartment building and public market, respectively.

black circles of Fig. 6 show that the integration results can compensate the missing blocks of MVAIs, but we should note that if these blocks exist in both UDIs and MVAIs, they will also exist in the integration results (red circles).

3) Summary: From the usability analysis, we can observe that the stitching errors of NIPIs lead to a quality loss in 3DSR and 3DPCs. Although NIPIs with the longest SR length (i.e., NIPI-20) can achieve comparatively good results, it is still unsatisfactory for accurate 3-D mapping. However, when integrating NIPIs and MVAIs, the results can not only compensate the stitching errors of NIPIs to yield a more accurate result, but also improve the completeness of MVAIs. Compared to the reference data, the integration results are acceptable and have high data processing efficiency for 3DPCs generation, which means it is applicable for rapid damage area measurement.

V. Conclusion

Many studies have used MVAIs for damaged areas classi-fication, while the generated 3DPCs are essential information for improving the detection reliability. However, since the MVAIs are poorly suited to observe damage at a building's lower floor in densely built-up areas, GPIs are required to compensate the viewpoint difference and to record the ground failure structure. In this study, we used a small UAV and a BPIS to collect both MVAIs and GPIs of two collapsed buildings, and integrated them for 3DPCs analysis. Since the stitching errors of GPIs result in NIPIs, we conducted a series of usability analysis of 3DPCs. The analysis showed that even

though the integration results experienced an accuracy loss in 3DPCs, they also showed advantages of high data process-ing efficiency and the ability to yield more complete 3DPCs than MVAIs. Therefore, in order to achieve a comprehensive and rapid building damage investigation, it is indispensable to jointly utilize MVAIs and GPIs to make up for each other's drawbacks in 3-D mapping.

References

[1] N. Kerle, F. Nex, M. Gerke, D. Duarte, and A. Vetrivel, "UAV-based structural damage mapping: A review," *ISPRS Int. J. Geo-Inf.*, vol. 9, no. 1, p. 14, Dec. 2019.

[2] F. Remondino, M. G. Spera, E. Nocerino, F. Menna, and F. Nex, "State of the art in high density image matching," *Photogramm. Rec.*, vol. 29, no. 146, pp. 144–166, Jun. 2014.

[3] A. Vetrivel, M. Gerke, N. Kerle, and G. Vosselman, "Identification of damage in buildings based on gaps in 3D point clouds from very high resolution oblique airborne images," *ISPRS J. Photogramm. Remote Sens.*, vol. 105, pp. 61–78, Jul. 2015.

[4] A. Vetrivel, M. Gerke, N. Kerle, F. Nex, and G. Vosselman, "Disaster damage detection through synergistic use of deep learning and 3D point cloud features derived from very high resolution oblique aerial images, and multiple-kernel-learning," *ISPRS J. Photogramm. Remote Sens.*, vol. 140, pp. 45–59, Jun. 2018.

[5] J. F. Galarreta, N. Kerle, and M. Gerke, "UAV-based urban structural damage assessment using object-based image analysis and semantic rea-soning," *Natural Hazards Earth Syst. Sci.*, vol. 15, no. 6, pp. 1087–1101, Jun. 2015.

[6] G. Petrie, "Mobile mapping systems: An introduction to the technology," *Geoinformatics*, vol. 13, no. 1, pp. 32–43, 2010.

[7] D. Turner, A. Lucieer, and L. Wallace, "Direct georeferencing of ultrahigh-resolution UAV imagery," *IEEE Trans. Geosci. Remote Sens.*, vol. 52, no. 5, pp. 2738–2745, May 2014.

[8] G. Pintore, R. Pintus, F. Ganovelli, R. Scopigno, and E. Gobbetti, "Recovering 3D existing-conditions of indoor structures from spherical images," *Comput. Graph.*, vol. 77, pp. 16–29, Dec. 2018.

[9] D. Anguelov *et al.*, "Google street view: Capturing the world at street level," *Computer*, vol. 43, no. 6, pp. 32–38, Jun. 2010.

[10] J. Y. Rau, B. W. Su, K. W. Hsiao, and J. P. Jhan, "Systematic calibration for a backpacked spherical photogrammetry imaging system," *ISPRS Int. Arch. Photogramm., Remote Sens. Spatial Inf. Sci.*, vol. 41, pp. 695–702, Jun. 2016.

[11] J. P. Jhan, J. Y. Rau, N. Haala, and M. Cramer, "Investigation of parallax issues for multi-lens multispectral camera band co-registration," *ISPRS Int. Arch. Photogramm., Remote Sens. Spatial Inf. Sci.*, vol. 42, pp. 157–163, Aug. 2017.

[12] G. Fangi and C. Nardinocchi, "Photogrammetric processing of spher-ical panoramas," *Photogramm. Rec.*, vol. 28, no. 143, pp. 293–311, Sep. 2013.

[13] S. Ji *et al.*, "Comparison of two panoramic sensor models for precise 3D measurements," *Photogramm. Eng. Remote Sens.*, vol. 80, no. 3, pp. 229–238, Mar. 2014.

[14] Y.-H. Tseng, Y.-C. Chen, and K.-Y. Lin, "Bundle adjustment of spherical images acquired with a portable panoramic image mapping system (PPIMS)," *Photogramm. Eng. Remote Sens.*, vol. 82, no. 12, pp. 935–943, Dec. 2016.

[15] S. J. Lee, T. Y. Yeh, and Y. Y. Lin, "Anomalously large ground motion in the 2016 ML 6.6 Meinong, Taiwan, earthquake: A synergy effect of source rupture and site amplification," *Seismol. Res. Lett.*, vol. 87, no. 6, pp. 1319–1326, 2016.

[16] J. Cusicanqui, N. Kerle, and F. Nex, "Usability of aerial video footage for 3-D scene reconstruction and structural damage assessment," *Natural Hazards Earth Syst. Sci.*, vol. 18, no. 6, pp. 1583–1598, Jun. 2018.

[17] M. Brown and D. G. Lowe, "Automatic panoramic image stitching using invariant features," *Int. J. Comput. Vis.*, vol. 74, no. 1, pp. 59–73, Apr. 2007.

[18] D. Jarron, M. Shahbazi, D. Lichti, and R. Radovanovic, "Automatic detection and labelling of photogrammetric control points in a calibration test field," *ISPRS Int. Arch. Photogramm., Remote Sens. Spatial Inf. Sci.*, vols. XLII-2/W13, pp. 1673–1680, Jun. 2019.

[19] P. Fanta-Jende, F. Nex, G. Vosselman, and M. Gerke, "Co-registration of panoramic mobile mapping images and oblique aerial images," *Photogramm. Rec.*, vol. 34, no. 166, pp. 148–173, Jun. 2019.